



HAL
open science

Eddy-Induced Temperature and Salinity Variability in the Arabian Sea

Corinne Trott, Bulusu Subrahmanyam, Alexis Chaigneau, Heather Roman-Stork

► **To cite this version:**

Corinne Trott, Bulusu Subrahmanyam, Alexis Chaigneau, Heather Roman-Stork. Eddy-Induced Temperature and Salinity Variability in the Arabian Sea. *Geophysical Research Letters*, 2019, 46 (5), pp.2734-2742. 10.1029/2018GL081605. hal-04430654

HAL Id: hal-04430654

<https://hal.science/hal-04430654>

Submitted on 1 Feb 2024

HAL is a multi-disciplinary open access archive for the deposit and dissemination of scientific research documents, whether they are published or not. The documents may come from teaching and research institutions in France or abroad, or from public or private research centers.

L'archive ouverte pluridisciplinaire **HAL**, est destinée au dépôt et à la diffusion de documents scientifiques de niveau recherche, publiés ou non, émanant des établissements d'enseignement et de recherche français ou étrangers, des laboratoires publics ou privés.

Geophysical Research Letters

RESEARCH LETTER

10.1029/2018GL081605

Special Section:

New Understanding of the
Arabian Sea Circulation

Key Points:

- An eddy tracking algorithm was applied in the Arabian Sea, then sea surface temperature and salinity characteristics were analyzed
- Subsurface- and surface-intensified eddies were found, and we note a clear dominance of surface-intensified eddies
- Composites of anticyclonic (cyclonic) eddies throughout the surface and mixed layer provide insight to each type of eddy structure

Supporting Information:

- Supporting Information S1

Correspondence to:

C. B. Trott,
ctrott@seoe.sc.edu

Citation:

Trott, C. B., Subrahmanyam, B., Chaigneau, A., & Roman-Stork, H. L. (2019). Eddy-induced temperature and salinity variability in the Arabian Sea. *Geophysical Research Letters*, *46*, 2734–2742. <https://doi.org/10.1029/2018GL081605>

Received 6 DEC 2018

Accepted 14 FEB 2019

Accepted article online 19 FEB 2019

Published online 12 MAR 2019

Eddy-Induced Temperature and Salinity Variability in the Arabian Sea

Corinne B. Trott¹ , Bulusu Subrahmanyam¹ , Alexis Chaigneau^{2,3,4} , and Heather L. Roman-Stork¹ 

¹School of the Earth, Ocean, and Environment, University of South Carolina, Columbia, SC, USA, ²LEGOS, University of Toulouse, CNES, CNRS, IRD, UPS, Toulouse, France, ³Institut de Recherches Halieutiques et Océanologiques du Bénin (IRHOB), Cotonou, Benin, ⁴International Chair in Mathematical Physics and Applications (ICMPA–UNESCO Chair), University of Abomey-Calavi, Cotonou, Benin

Abstract The eddy field in the Arabian Sea experiences seasonal wind-driven intensification during the summer monsoon season from June through September. These strong eddies strengthen local currents like the Somali Current and strongly impact regional upper-level vertical and lateral advection. To investigate the multivariate response to eddying, we apply a closed-contour eddy-tracking algorithm to sea level anomaly maps and then examine sea surface temperature and salinity of the identified eddies to infer whether they are surface or subsurface intensified in the Arabian Sea during the summer monsoon. A complete understanding of the temperature and salinity signatures reveals how Arabian Sea eddies alter upper-ocean stratification. Though both intensification types are identified, we find a dominance of likely surface-intensified eddies characterized by relatively warm and fresh cores for anticyclonic eddies and relatively cool and saline cores for cyclonic eddies, particularly in the northwestern Arabian Sea and Somali Current region.

Plain Language Summary Mesoscale eddies in the ocean, analogous to their atmospheric cyclone and anticyclone counterparts, play a major role on the transport and redistribution of oceanic properties like heat or salt. They are highly variable and transient, so to fully understand their behavior, eddy tracking algorithms are typically used to identify these features and follow their trajectories. In this study, we apply an algorithm to sea level anomalies in order to track eddy formation, distribution, and duration during the summer monsoon season in the Arabian Sea. In sea surface height, cyclonic (anticyclonic) eddies appear as low (high) sea level anomalies. Though the overall displacement of the eddy can be estimated with sea level anomalies alone, a more in-depth investigation of the temperature and salinity at the surface and subsurface can provide insight to the vertical structure of the eddy. More specifically, a multiparameter approach allows for investigation of whether an eddy intensifies at or below the surface. This research analyzes the characteristics of eddies in the Arabian Sea during the southwest monsoon seasons from 2015 to 2018.

1. Introduction

During the summer monsoon season from June through September, a strong low-level southwesterly jet forms over the western Arabian Sea (Findlater, 1977). This jet (called the Findlater Jet; see Figure 1) induces surface turbulence that amplifies the strength of the local eddy field. The generation mechanism of these eddies is primarily wind driven, with secondary influences of Rossby waves and local barotropic instabilities (Jensen, 2001; McCreary et al., 1993; Trott et al., 2017). These eddies transport oceanic properties and mainly drive local upwelling and downwelling (Boccaletti et al., 2007). As a result, mesoscale eddies can have a distinct sea surface temperature (SST) footprint characterized by local extrema (Dong et al., 2011).

A multitude of algorithms have been developed to monitor the formation, propagation, characteristics, and dissipation of mesoscale eddies. Due to the availability of satellite-derived altimetric observations from 1993 to present and the well-studied relationship between sea level anomalies (SLAs) and geostrophic currents, most global eddy tracking algorithms have exclusively utilized gridded SLA fields (Chaigneau et al., 2008; Chelton et al., 2011; Williams et al., 2011; Yi et al., 2014). However, a more complete analysis requires consideration of other parameters such as SST and sea surface salinity (SSS), which can have local impacts on ocean stirring and mixing processes (Dong et al., 2011; d'Ovidio et al., 2004; Mukiibi et al., 2016; Pasquero,

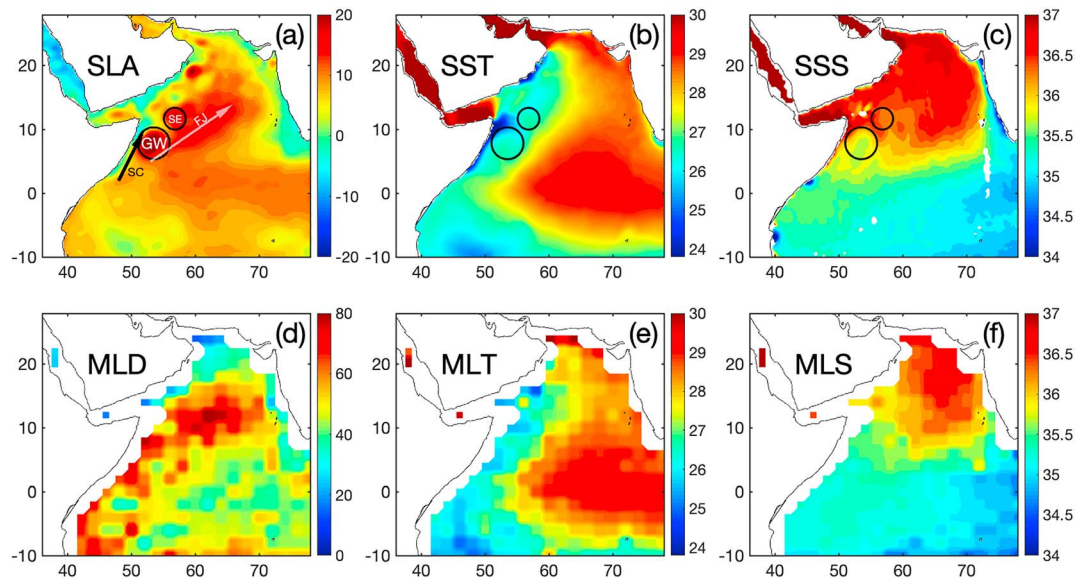


Figure 1. Climatological (a) sea level anomaly (SLA; in cm), (b) sea surface temperature (SST; in °C), (c) sea surface salinity (SSS), (d) mixed layer depth (MLD; in m), (e) mixed layer temperature (MLT; in °C), and (f) mixed layer salinity (MLS) for the southwest monsoon seasons from 2015 to 2018. The Great Whirl (GW), Socotra Eddy (SE), Somali Current (SC), and Findlater Jet (FJ) are delineated on the first panel, and the GW and SE locations are superimposed on all surface plots.

2005). Before the satellite era, the salinity and temperature characteristics of Arabian Sea eddies relied on survey observations (Fischer et al., 1996; Schott & Garternicht, 1997). However, since 1 April 2015, National Aeronautics and Space Administration (NASA)'s Soil Moisture Active Passive (SMAP) mission provides SSS with higher accuracy and swath coverage than any previous SSS missions and permits for the study of SSS eddy characteristics. Recent studies have also investigated the eddy signature on SSS in other parts of the world's oceans (e.g., Amores et al., 2018; Delcroix et al., 2019; Melnichenko et al., 2017).

Mesoscale eddies can be separated into four categories based on their rotation (cyclonic or anticyclonic) and whether they are intensified in the surface mixed layer or in subsurface layers (Assassi et al., 2016). A surface-intensified eddy has its core, characterized by a maximum potential vorticity, located within the mixed layer, whereas a subsurface-intensified eddy refers to an eddy having a maximum rotation and potential vorticity below the mixed layer (Assassi et al., 2016). Described well by Zhang et al. (2016), surface-intensified anticyclonic eddies have the largest deformation of isopycnals at the surface while those intensified at the subsurface are domed above the center and depressed below it. Likewise, subsurface-intensified cyclones have a depressed isopycnal shape above and a domed shape below (Assassi et al., 2016). Some examples of anticyclonic subsurface-intensified eddies include mode-water eddies (McGillicuddy et al., 2007), intrathermocline eddies (Chaigneau et al., 2011; Hormazabal et al., 2013; Kostianoy & Belkin, 1989; Meunier et al., 2018), and mixed layer subduction from air-sea fluxes (Zhang et al., 2016). Subsurface-intensified cyclonic eddies have also been observed in regions like the southeastern Baltic Sea (Zhurbas et al., 2004). In upwelling regions driven by a constant wind along a coastal region (such as the western Arabian Sea), McGillicuddy (2015) identified the development of both surface- and subsurface-intensified eddies, conjectured to be due to local adiabatic processes, barotropic and baroclinic instabilities, or topographic influences (Badin et al., 2011; Draeger et al., 2018; Marchesiello et al., 2010; Meunier et al., 2010; Morel et al., 2006; Thomas, 2008). Fortunately, a comparison between SLA and SST anomalies provided insight to the subsurface structure and intensification dynamics of mesoscale eddies (Assassi et al., 2016; Bashmachnikov et al., 2013; Caballero et al., 2008). The dynamical investigation conducted in this research is inspired by the a priori relationship between SLA and SST anomalies determined by Assassi et al. (2016) that allows for the differentiation between surface- and subsurface-intensified eddies from surface satellite observations only. We take advantage of the high quality and coverage of NASA's SMAP mission to expound on the SSS signature of each eddy type. This research aims to quantify and explore how eddies in the Arabian Sea impact temperature and salinity anomalies at the surface and throughout the mixed layer.

In the era of big data, manual analysis of transient and small-scale features such as eddies is impractical and inefficient. The useful application of an automatic eddy tracking method to SLA fields and then an investigation into the physical properties of the detected eddies motivate this research. The objective of this study is to better quantify the spatial and temporal characteristics of surface- and subsurface-intensified anticyclonic and cyclonic eddies in the Arabian Sea during the summer monsoon seasons from 2015 to 2018 (to align with the temporal coverage of NASA's SMAP mission).

2. Data and Methodology

Altimetric SLAs used in this research are provided and maintained by the Copernicus Marine and Environment Monitoring Service (marine.copernicus.eu). This daily product is available at a 0.25° global horizontal grid resolution and integrates observations from multiple altimeters (Ducet et al., 2000; Le Traon et al., 1998). An advantage of altimetry is that it does not experience signal contamination from cloud cover because it possesses an active sensor, which is advantageous in eddy studies.

SST is from the Optimum Interpolation Sea Surface Temperature V2 data set from the Advanced Very High Resolution Radiometer developed by the National Oceanic and Atmospheric Administration and the National Climatic Data Center (Reynolds et al., 2007) at a 0.25° global horizontal grid resolution. Also, at the same horizontal resolution, SSS in this study is from NASA's SMAP mission. We used NASA's Jet Propulsion Lab's version 4.0 CAP data, which uses SMAP's exact 8-day orbit repeat cycle (though SMAP has near global coverage every 3 days) to produce daily files from the 8-day running mean. This version accounts for reduced brightness temperature biases and integrates galaxy and land contamination corrections (Fore et al., 2016).

To observe the subsurface response to the detected eddies, the Mixed layer data set of Argo, Grid Point Value product was developed and provided by Japan Agency for Marine-Earth Science and Technology. This product contains gridded mixed layer depths (MLDs) and its related temperatures and salinities in 10-day intervals from Argo float data, which have good coverage in the Arabian Sea region (Hosoda et al., 2010). The mixed layer product selected uses a 0.125 kg/m^3 density threshold, which has been shown to be an appropriate MLD criteria in this region (Suga et al., 2004; Trott et al., 2017). Each Argo profile is quality controlled as described in Hosoda et al. (2010).

The eddy tracking method used in Pegliasco et al. (2015) and Trott et al. (2018) was applied to SLA. First, individual eddies are identified in each daily gridded SLA field by a center and an edge (Chaigneau et al., 2008, 2009). Positive (negative) anomalies in SLA were identified as anticyclonic (cyclonic) eddies. The outermost closed contour around the center is defined as the eddy edge. This method detects a lower number of false eddies than alternative methods (Chaigneau et al., 2008; Chelton et al., 2011; Souza et al., 2011; Yi et al., 2014). Additionally, there is no thresholding of eddies based on arbitrary criteria (Chaigneau et al., 2008; Chelton et al., 2011), and this method produces a more accurate eddy shape.

Eddy property anomalies for sea-surface temperature anomaly (SSTA), sea-surface salinity anomaly (SSSA), mixed layer depth anomaly (MLDA), mixed layer temperature anomaly (MLTA), and mixed layer salinity anomaly (MLSA) were computed as follows. First, for each eddy, its mean properties are computed averaging each parameter between the eddy center and one radius. Second, anomalies are computed relative to the corresponding surrounding properties averaged between one radius and three radii from the eddy center. Warm-core (cold-core) eddies are associated with positive (negative) SST anomalies.

3. Results

During the summer monsoon season, the Findlater Jet and its associated wind stress synergize with the topography of the Somali coastline to induce strong upwelling (Trott et al., 2017). Upwelled waters are then recirculated by large-scale circulation and mesoscale features. Climatological summer SLA (Figure 1a) clearly reveals strong quasi-permanent eddies like the Great Whirl around 52°E and 9°N and the Socotra Eddy to its northeast (Akueteve et al., 2016; Beal & Donohue, 2013; Trott et al., 2018; Figure 1a,b). Additionally, the SSS field reveals low salinity values within the Great Whirl with the Arabian Sea high salinity water mass about its exterior (Beal & Donohue, 2013; Figure 1c). Meanwhile, lower salinity waters are advected north-eastward via the Somali Current, which outflows into the high-salinity Arabian Sea water mass (Figure 1c).

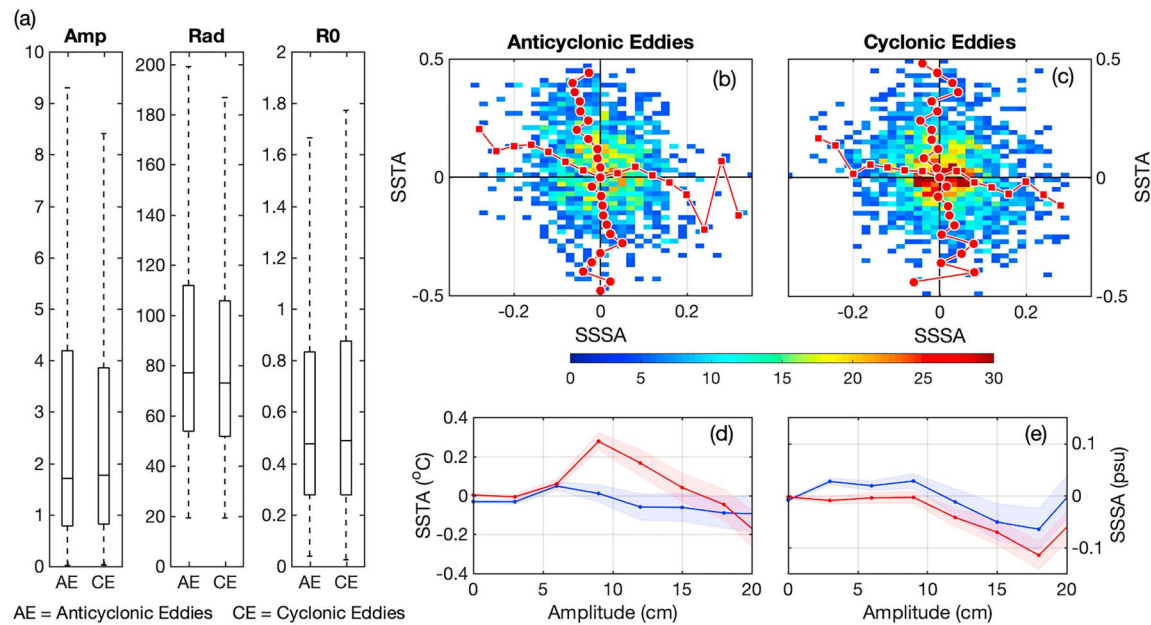


Figure 2. Boxplots (a) showing distribution of eddy amplitudes (cm), radii (km), and Rossby number. Upper panels show the binned bidimensional relationship between sea surface temperature anomaly (SSTA) and sea surface salinity anomaly (SSSA) for each eddy with average SSTA in red squares and average SSSA in red circles (b and c). Frequencies lower than five eddies have been removed. Bottom panels show the relationship between amplitude and SSTA/SSSA for anticyclonic (red) and cyclonic (blue) eddies (d and e). Normalized error is shaded.

The pattern of high MLDs in the Arabian Sea mirrors the spatial distribution of the Findlater Jet (Findlater, 1977) and intensifies along the Somali Current outflow region and the central Arabian Sea basin (Figure 1). The MLD in the Arabian Sea was approximately 70–80 m deep along the axis of the Findlater Jet and otherwise had a depth of approximately 40 m (Figure 1d). The temperature and salinity spatial distributions averaged throughout the mixed layer similarly (MLT and MLS, respectively) reflect those of SST and SSS, clearly delineating the upwelling extent and revealing slightly lower salinities than the surface (Figure 1). However, some weak differences are observed, probably due to (i) the difference in the spatiotemporal resolution of the data sets and (ii) the satellite data that are determined from the characteristics of the skin layer corresponding to the upper ~1 cm while that in Argo profiles corresponds to the first few meters.

To directly compare the surface characteristics of the detected eddies, their amplitudes, radii, Rossby numbers (R_0), and average SSS and SST characteristics were determined for each eddy detected during summer monsoon periods of 2015–2018. Eddy amplitudes and eddy characteristics are skewed and favor smaller radii and amplitudes (Figure 2). The total number of closed-contour eddies during the four summer monsoon seasons is of 23,639 for anticyclonic eddies and 25,599 for cyclonic eddies. Figure 2 displays the average distribution of the eddy characteristics for each summer monsoon season (June through September). The highest frequency amplitude of cyclonic (anticyclonic) eddies for each monsoon season (June through September) was about 0.3 cm with ~750 (730) eddies per year. The median amplitude for both cyclonic and anticyclonic eddies was slightly below 2 cm, and there was larger skewing of anticyclonic eddies to favor larger amplitudes. Cyclonic eddies tended to have warmer SSTA and more saline SSSA than anticyclonic eddies. Radii were overall slightly larger for anticyclonic eddies than cyclonic eddies, which likely influenced the higher Rossby number for cyclonic eddies as they had smaller length scales. A majority of values for the identified eddies was between 0.3 and 0.8, consistent with the theoretical studies of Badin (2013) and Ragone and Badin (2016), and suggesting that ageostrophic processes can be important for the Arabian Sea eddies. Though the spread of SSSA and SSTA ranges approximately between ± 0.2 salinity units and ± 0.4 °C (Figures 2b and 2c), the vast majority of eddies have very small anomalies, hence the small amplitudes in the amplitude-anomaly relationship in Figures 2d and 2e.

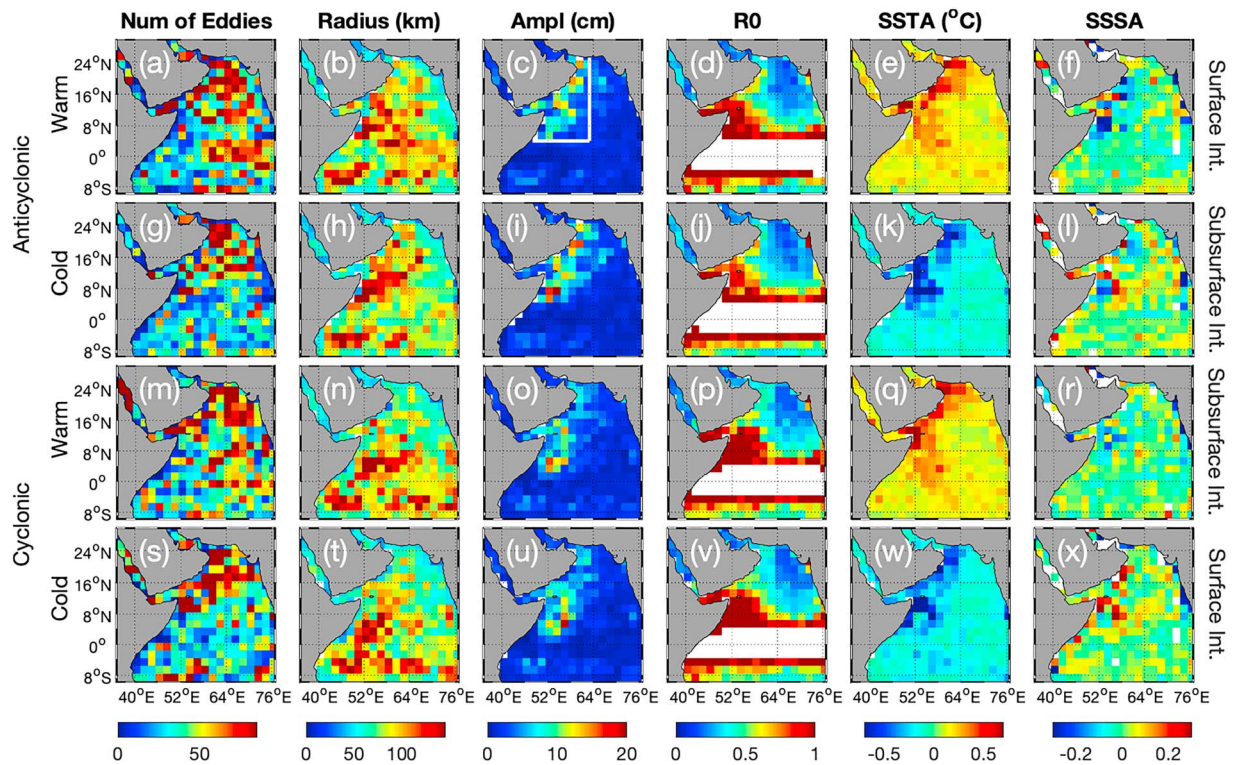


Figure 3. Mean spatial distribution of eddy characteristics during summer monsoon season (June–September) from 2015 through 2018. Characteristics are (left to right) number of eddies (panels a, g, m, s), radius (panels b, h, n, t), amplitude (panels c, i, o, u), Rossby number (panels d, j, p, v), sea surface temperature anomaly (SSTA; panels e, k, q, w), and sea surface salinity anomaly (SSSA; panels f, l, r, x). For each row, eddies were classified whether anticyclonic and cyclonic eddies were associated with warm (SSTA > 0) or cold (SSTA < 0) cores. Likely intensification type is labeled along the right y-axis.

The spatial distribution of the characteristics of the detected eddies is unique for not only each type of eddy when categorized by sense of rotation, but also when separated by warm and cold-core eddies (Figure 3). The distinction between warm and cold-core eddies is used to separate, as a first guess, the surface- and subsurface-intensified eddies. Regardless of SLA or SSTA, the highest number of eddies for all eddy types is observed in the northern Arabian Sea (Figure 3). The mean radii, however, show some spatial variation. Anticyclonic warm-core and cyclonic cold-core eddies, both likely associated with surface-intensified eddies (Assassi et al., 2016), revealed the highest mean radii in the location of the Great Whirl and its surrounding eddy field. Though the lateral distribution of upwelled waters is strongly a function of eddy-induced advection, the intensity of SSTA is also reliant on the magnitude of upwelling, typically identified by summer monsoon season strength (Figure 3). The largest radii for all eddy types are evenly distributed along the central and southern Arabian Sea, with observed peaks in the Great Whirl region. The region of largest eddies is shifted more northward in the distribution of warm-core anticyclonic eddies than warm-core cyclonic eddies, though both are along the Somali Current (Figures 3c and 3o). The highest amplitude eddies are associated with Somali Current outflow and upwelling along the Arabian Peninsula. The highest SSTAs (+/−0.5 to 0.7 °C) coincide with the highest amplitude eddies, more specifically for anticyclones. For both anticyclonic and cyclonic eddies, the warm (cold) core eddies tended to be fresher (saltier). The clearest spatial relationship between SSTA and SSSA for eddies was for anticyclonic warm-core and cyclonic cold-core eddies, which are likely surface intensified (Figure 3). Note that the relationship between SSTA and SSSA held true when eddies are classified using their SSSA instead of SSTA as done in Figure 3 (Figure S1 in the supporting information). This is due to the vertical salinity structure in the northwestern Arabian Sea, which not only possesses a strong zonal salinity gradient between the equatorially sourced waters of the Somali Current and the high salinity Arabian Sea water mass but also experiences a subsurface salinity maximum (Figure S2).

To better understand the impact of each type of eddy on the upper water-column characteristics, composite analyses were conducted considering the most energetic region (west of 63°E and north of 4°N, delineated in Figure 3c) associated with high-amplitude eddies. Composites were normalized by eddy radius to accurately

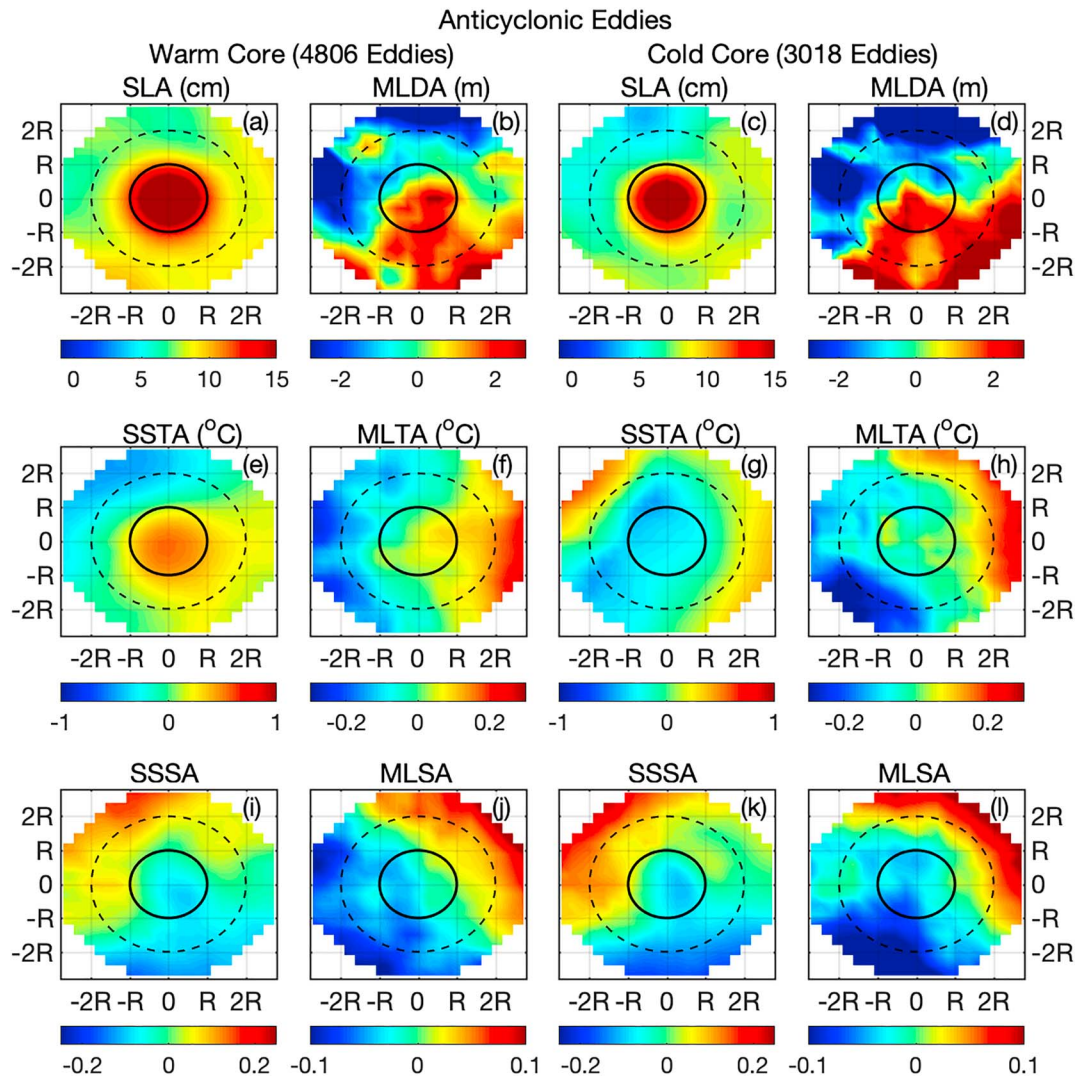


Figure 4. Composites of warm and cold-core anticyclonic eddies west of 63°E and north of 4°N. SLA (panels a,c), MLDA (panels b, d), SSTA (panels e,g), MLTA (panels f, h), SSSA (panels i, k), MLSA (panels j, l). MLDA = mixed layer depth anomaly, MLTA = mixed layer temperature anomaly; SSTA = sea surface temperature anomaly; SSSA = sea surface salinity anomaly.

describe the structure of each eddy type. When separating the anticyclonic eddies by warm and cold-core type (using $SSTA > 0$ or $SSTA < 0$), the amplitude of the mean SSTA is similar and of ± 0.1 °C (Figures 4e and 4g) but is extended to the southwest of the eddy in the cold-core composites and extended slightly southeast in the warm-core composites. Interestingly, both warm and cold-core anticyclonic eddies have a similar SSSA signal (Figures 4i and 4k), both in magnitude and in spatial distribution, tending to have a fresh core, anomalously fresh waters to the south, and anomalously saline waters to the north. This pattern is seen in MLSA to be shifted clockwise 90° (Figures 4j and 4l). In MLTA, there is an eastward increasing temperature in warm-core eddies with a positive temperature anomaly within one eddy radius (Figure 4f). The MLTA in cold-core eddies is very weak, with cooler waters to the south and west and warmer waters to the north and east (Figure 4h). Interestingly, the MLDA is similar for warm-core and cold-core anticyclonic eddies (Figures 4b and 4d), though it would be expected to see deepening in surface-intensified anticyclones and shallowing in subsurface-intensified anticyclones.

Composites of cyclonic eddies were constructed (Figure 5) and compared with those of anticyclonic eddies. The results indicate that there is more difference in mixed layer and SSS characteristics in the Arabian Sea between cyclones and anticyclones than when cyclonic and anticyclonic eddies are separated into warm and cold cores. Like their anticyclonic counterparts, the magnitude of the composite warm and cold-core

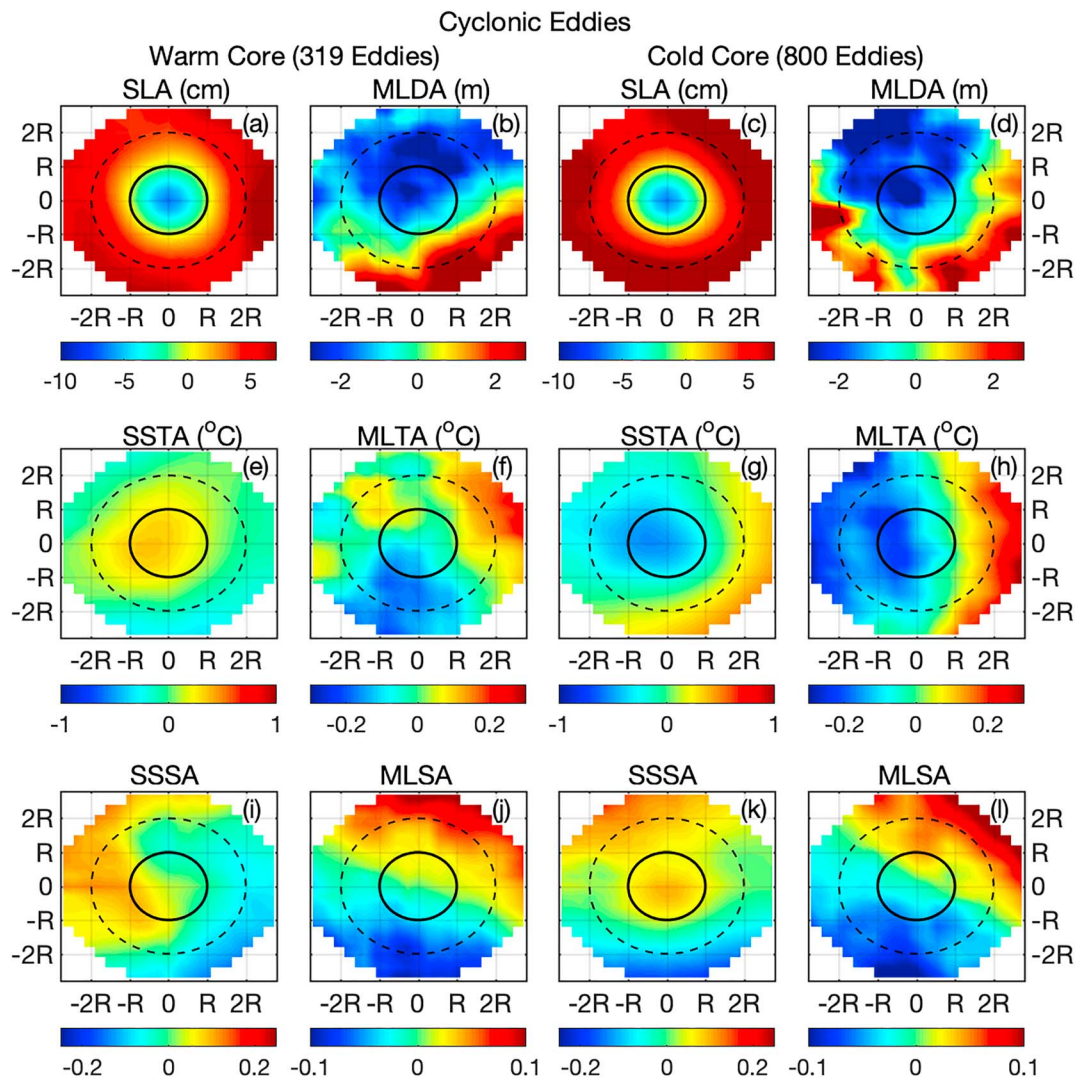


Figure 5. Same as Figure 4, but for cyclonic eddies. SLA (panels a,c), MLDA (panels b, d), SSTA (panels e,g), MLTA (panels f, h), SSSA (panels i, k), MLSA (panels j, l).

temperature anomaly is approximately the same, but in the case of cyclonic eddies, the SSTA center is skewed to the southwest for warm-core eddies and to the northwest for cold-core eddies. The MLTA distribution between warm and cold-core eddies is opposite that of anticyclonic eddies: where anticyclonic warm-core eddies have an eastward gradient seen in the cold-core cyclonic eddies and anticyclonic cold-core eddies have a northeastward MLTA gradient like that seen in cyclonic warm-core eddies. The MLSA is distributed similar in cyclonic eddies to anticyclonic eddies, but there is a notable difference in SSSA. The anticyclonic eddies (of all temperature core types) are anomalously fresh within one radius; however, the composites of both types of cyclonic eddies reveal anomalously high salinity centers, feeding in to the center of the eddy from the west in warm-core cyclonic eddies and from the north in cold-core cyclonic eddies.

4. Conclusions

The eddy field in the Arabian Sea experiences high variability, particularly during the summer monsoon season from June through September as a response to strong low-level wind forcing. This research builds upon the current literature of eddy study in the Arabian Sea by exploring the characteristics of SST and SSS at the surface and throughout the mixed layer. We apply a closed SLA contour eddy tracking algorithm and explore

the SST and SSS signatures of the detected eddies. A total of 23,639 anticyclonic and 25,599 cyclonic eddies were identified and investigated. They were compared in terms of amplitude, radius, SSTA, SSSA, and mixed layer depth, temperature, and salinity anomalies. The highest number of detected eddies was in the northern Arabian Sea, and the most robust, high-amplitude eddies were found in the Somali Current outflow region and off the coast of the Arabian Peninsula. Separation of the mean spatial characteristics of anticyclonic and cyclonic eddies when separated by warm and cold cores revealed an overall higher frequency of warm-core anticyclonic and cold-core cyclonic eddies, both of which are likely associated with surface intensification. This research identified the relevant eddy-driven salinity signature, finding the warm-core anticyclonic eddies to be anomalously fresh and the cold-core cyclonic eddies to be anomalously saline. The relationship also held true when filtering by fresh and saline core eddies. In a composite analysis, the fresh cores were associated with anticyclonic eddies, even when separated into warm and cold-core eddies. The opposite was true in the composite of cyclonic eddies, which showed to have positive SSSA cores. The surface and subsurface characteristics were not confirmed in the MLDA, which always reflected a deepening (shallowing) of ~3 m in anticyclones (cyclones).

In the context of monsoonal air-sea interactions, eddying in the Arabian Sea is integral to altering local mixed layer stratification. The moisture source for the heavy rainfall associated with the Indian summer monsoon is sourced from over the Arabian Sea and advected by the Findlater Jet. Further investigation into the temperature and salinity characteristics of eddies in the Arabian Sea and how they change from year to year is integral to air-sea fluxes, particularly in the case of barrier layer development by increased eddy-induced transfer of freshwater (Thadathil et al., 2008).

Acknowledgments

This work is supported by the ONR NASCar (Northern Arabian Sea Circulation-autonomous research) award N00014-15-1-2591, awarded to B. S. SLA are provided by the Copernicus Marine Environmental Monitoring Service (CMEMS; marine.copernicus.eu). SST data access and further description are available via the NOAA website (ncdc.noaa.gov/oisst). SSS used in this research is available via NASA's Jet Propulsion Lab Physical Oceanography Distributed Active Archive Center (podaac.jpl.nasa.gov). The authors would like to thank the anonymous reviewers and the editor, whose comments significantly contributed to the improvement of this paper.

References

- Akueteve, C. Q. C., Barnier, B., Verron, J., Molines, J. M., & Lecointre, A. (2016). Interactions between the Somali Current eddies during the summer monsoon: Insights from a numerical study. *Ocean Science*, *12*(1), 185–205. <https://doi.org/10.5194/os-12-185-2016>
- Amores, A., Jordà, G., Arsouze, T., & Le Sommer, J. (2018). Up to what extent can we characterize ocean eddies using present-day gridded altimetric products? *Journal of Geophysical Research: Oceans*, *123*(10), 7220–7236. <https://doi.org/10.1029/2018JC014140>
- Assassi, C., Morel, Y., Vandermeersch, F., Chaigneau, A., Pegliasco, C., Morrow, R., et al. (2016). An index to distinguish surface- and subsurface-intensified vortices from surface observations. *Journal of Physical Oceanography*, *46*(8), 2529–2552. <https://doi.org/10.1175/JPO-D-15-0122.1>
- Badin, G. (2013). Surface semi-geostrophic dynamics in the ocean. *Geophysical and Astrophysical Fluid Dynamics*, *107*(5), 526–540. <https://doi.org/10.1080/03091929.2012.740479>
- Badin, G., Tandon, A., & Mahadevan, A. (2011). Lateral mixing in the pycnocline by baroclinic mixed layer eddies. *Journal of Physical Oceanography*, *41*(11), 2080–2101. <https://doi.org/10.1175/JPO-D-11-05.1>
- Bashmachnikov, I., Boutov, D., & Dias, J. (2013). Manifestation of two meddies in altimetry and sea-surface temperature. *Ocean Science*, *9*(2), 249–259. <https://doi.org/10.5194/os-9-249-2013>
- Beal, L. M., & Donohue, K. A. (2013). The Great Whirl: Observations of its seasonal development and interannual variability. *Journal of Geophysical Research: Oceans*, *118*, 1–13. <https://doi.org/10.1029/2012JC008198>
- Boccaletti, G., Ferrari, R., & Fox-Kemper, B. (2007). Mixed layer instabilities and restratification. *Journal of Physical Oceanography*, *37*(9), 2228–2250. <https://doi.org/10.1175/JPO3101.1>
- Caballero, A., Pascual, A., Dibarboure, G., & Espino, M. (2008). Sea level and Eddy kinetic energy variability in the Bay of Biscay, inferred from satellite altimeter data. *Journal of Marine Systems*, *72*(1–4), 116–134. <https://doi.org/10.1016/j.jmarsys.2007.03.011>
- Chaigneau, A., Eldin, G., & Dewitte, B. (2009). Eddy activity in the four major upwelling systems from satellite altimetry (1992–2007). *Progress in Oceanography*, *83*(1–4), 117–123. <https://doi.org/10.1016/j.pocean.2009.07.012>
- Chaigneau, A., Gizolme, A., & Grados, C. (2008). Mesoscale eddies off Peru in altimeter records: Identification algorithms and eddy spatio-temporal patterns. *Progress in Oceanography*, *79*(2–4), 106–119. <https://doi.org/10.1016/j.pocean.2008.10.013>
- Chaigneau, A., Le Texier, M., Eldin, G., Grados, C., & Pizarro, O. (2011). Vertical structure of mesoscale eddies in the eastern South Pacific Ocean: A composite analysis from altimetry and Argo profiling floats. *Journal of Geophysical Research*, *116*, C11025. <https://doi.org/10.1029/2011JC007134>
- Chelton, D. B., Schlax, M. G., & Samelson, R. M. (2011). Global observations of nonlinear mesoscale eddies. *Progress in Oceanography*, *91*(2), 167–216. <https://doi.org/10.1016/j.pocean.2011.01.002>
- Delcroix, T., Chaigneau, A., Sviadani, D., Boutin, J., & Pegliasco, C. (2019). Eddy-induced salinity changes in the tropical Pacific. *Journal of Geophysical Research: Oceans*, *124*(1), 374–389. <https://doi.org/10.1029/2018JC014394>
- Dong, C., Nencioli, F., Liu, Y., & McWilliams, J. C. (2011). An automated approach to detect oceanic eddies from satellite remotely sensed sea surface temperature data. *IEEE Geoscience and Remote Sensing Letters*, *8*(6), 1055–1059. <https://doi.org/10.1109/LGRS.2011.2155029>
- d'Ovidio, F., Fernández, V., Hernández-García, E., & López, C. (2004). Mixing structures in the Mediterranean Sea from finite-size Lyapunov exponents. *Geophysical Research Letters*, *31*, L17203. <https://doi.org/10.1029/2004GL020328>
- Draeger, J. G. K., Jochumsen, K., Griesel, A., & Badin, G. (2018). Relative dispersion of surface drifters in the Benguela upwelling region. *Journal of Physical Oceanography*, *48*(10), 2325–2341. <https://doi.org/10.1175/JPO-D-18-0027.1>
- Ducet, N., Le Traon, P. Y., & Reverdin, G. (2000). Global high-resolution mapping of ocean circulation from TOPEX/Poseidon and ERS-1 and-2. *Journal of Geophysical Research*, *105*(C8), 19,477–19,498. <https://doi.org/10.1029/2000JC900063>
- Findlater, J. (1977). A numerical index to monitor the Afro-Asian monsoon during the northern summers. *Meteorological Magazine*, *106*, 170–184.

- Fischer, J., Schott, F., & Stramma, L. (1996). Currents and transports of the Great Whirl-Socotra Gyre system during the summer monsoon, August 1993. *Journal of Geophysical Research*, *101*(C2), 3573–3587. <https://doi.org/10.1029/95JC03617>
- Fore, A. G., Yueh, S. H., Tang, W., Stiles, B. W., & Hayashi, A. K. (2016). Combined active/passive retrievals of ocean vector wind and sea surface salinity with SMAP. *IEEE Transactions on Geoscience and Remote Sensing*, *54*(12), 7396–7404. <https://doi.org/10.1109/TGRS.2016.2601486>
- Hormazabal, S., Combes, V., Morales, C. E., Correa-Ramirez, M. A., Di Lorenzo, E., & Nuñez, S. (2013). Intrathermocline eddies in the coastal transition zone off central Chile (31–41 S). *Journal of Geophysical Research: Oceans*, *118*, 4811–4821. <https://doi.org/10.1002/jgrc.20337>
- Hosoda, S., Ohira, T., Sato, K., & Suga, T. (2010). Improved description of global mixed layer depth using Argo profiling floats. *Journal of Oceanography*, *66*(6), 773–787. <https://doi.org/10.1007/s10872-010-0063-3>
- Jensen, T. G. (2001). Arabian Sea and Bay of Bengal exchange of salt and tracers in an ocean model. *Geophysical Research Letters*, *28*(20), 3967–3970. <https://doi.org/10.1029/2001GL013422>
- Kostianoy, A., & Belkin, I. (1989). A survey of observations on intrathermocline eddies in the world ocean. In J. Nihoul, & B. Jamart (Eds.), *Mesoscale/synoptic coherent structures in geophysical turbulence* (Vol. 50, pp. 821–841). New York: Elsevier. [https://doi.org/10.1016/S0422-9894\(08\)70223-X](https://doi.org/10.1016/S0422-9894(08)70223-X)
- Le Traon, P. Y., Nadal, F., & Ducet, N. (1998). An improved mapping method of multisatellite altimeter data. *Journal of Atmospheric and Oceanic Technology*, *15*(2), 522–534. [https://doi.org/10.1175/1520-0426\(1998\)015<0522:AIMMOM>2.0.CO;2](https://doi.org/10.1175/1520-0426(1998)015<0522:AIMMOM>2.0.CO;2)
- Marchesiello, P., Lefèvre, J., Vega, A., Couvelard, X., & Menkes, C. (2010). Coastal upwelling, circulation and heat balance around New Caledonia's barrier reef. *Marine Pollution Bulletin*, *61*(7–12), 432–448. <https://doi.org/10.1016/j.marpolbul.2010.06.043>
- McCreary, J. P. Jr., Kundu, P. K., & Molinari, R. L. (1993). A numerical investigation of dynamics, thermodynamics and mixed layer processes in the Indian Ocean. *Progress in Oceanography*, *31*(3), 181–244. [https://doi.org/10.1016/0079-6611\(93\)90002-U](https://doi.org/10.1016/0079-6611(93)90002-U)
- McGillicuddy, D. J. Jr. (2015). Formation of intrathermocline lenses by eddy-wind interaction. *Journal of Physical Oceanography*, *45*(2), 606–612. <https://doi.org/10.1175/JPO-D-14-0221.1>
- McGillicuddy, D. J., Anderson, L. A., Bates, N. R., Bibby, T., Buesseler, K. O., Carlson, C. A., et al. (2007). Eddy/wind interactions stimulate extraordinary mid-ocean plankton blooms. *Science*, *316*(5827), 1021–1026. <https://doi.org/10.1126/science.1136256>
- Melnichenko, O., Amores, A., Maximenko, N., Hacker, P., & Potemra, J. (2017). Signature of mesoscale eddies in satellite sea surface salinity. *Journal of Geophysical Research: Oceans*, *122*, 1416–1424. <https://doi.org/10.1002/2016JC012420>
- Meunier, T., Rossi, V., Morel, Y., & Carton, X. (2010). Influence of bottom topography on an upwelling current: Generation of long trapped filaments. *Ocean Modelling*, *35*(4), 277–303. <https://doi.org/10.1016/j.ocemod.2010.08.004>
- Meunier, T., Tenreiro, M., Pallàs-Sanz, E., Ochoa, J., Ruiz-Angulo, A., Portela, E., et al. (2018). Intrathermocline eddies embedded within an anticyclonic vortex ring. *Geophysical Research Letters*, *45*, 7624–7633. <https://doi.org/10.1029/2018GL077527>
- Morel, Y. G., Darr, D. S., & Talandier, C. (2006). Possible sources driving the potential vorticity structure and long-wave instability of coastal upwelling and downwelling currents. *Journal of Physical Oceanography*, *36*(5), 875–896. <https://doi.org/10.1175/JPO2899.1>
- Mukiibi, D., Badin, G., & Serra, N. (2016). Three dimensional chaotic advection by mixed layer baroclinic instabilities. *Journal of Physical Oceanography*, *46*(5), 1509–1529. <https://doi.org/10.1175/JPO-D-15-0121.1>
- Pasquero, C. (2005). Differential eddy diffusion of biogeochemical tracers. *Geophysical Research Letters*, *32*, L17603. <https://doi.org/10.1029/2005GL023662>
- Pegliasco, C., Chaigneau, A., & Morrow, R. (2015). Main eddy vertical structures observed in the four major eastern boundary upwelling systems. *Journal of Geophysical Research: Oceans*, *120*, 6008–6033. <https://doi.org/10.1002/2015JC010950>
- Ragone, F., & Badin, G. (2016). Surface semi-geostrophic turbulence: Freely-evolving dynamics. *Journal of Fluid Mechanics*, *792*, 740–774. <https://doi.org/10.1017/jfm.2016.116>
- Reynolds, R. W., Smith, T. M., Liu, C., Chelton, D. B., Casey, K. S., & Schlax, M. G. (2007). Daily high-resolution-blended analyses for sea surface temperature. *Journal of Climate*, *20*(22), 5473–5496. <https://doi.org/10.1175/2007JCLI1824.1>
- Schott, F., & Gartnericht, U. (1997). Heat fluxes of the Indian Ocean from a global eddy-resolving model. *Journal of Geophysical Research*, *102*(C9), 21,147–21,159.
- Souza, J. M. A. C. D., De Boyer Montegut, C., & Le Traon, P. Y. (2011). Comparison between three implementations of automatic identification algorithms for the quantification and characterization of mesoscale eddies in the South Atlantic Ocean. *Ocean Science*, *7*(3), 317–334. <https://doi.org/10.5194/os-7-317-2011>
- Suga, T., Motoki, K., Aoki, Y., & Macdonald, A. M. (2004). The North Pacific climatology of winter mixed layer and mode waters. *Journal of Physical Oceanography*, *34*(1), 3–22. [https://doi.org/10.1175/1520-0485\(2004\)034<0003:TNPCOW>2.0.CO;2](https://doi.org/10.1175/1520-0485(2004)034<0003:TNPCOW>2.0.CO;2)
- Thadathil, P., Thoppil, P., Rao, R. R., Muraleedharan, P. M., Somayajulu, Y. K., Gopalakrishna, V. V., et al. (2008). Seasonal variability of the observed barrier layer in the Arabian Sea. *Journal of Physical Oceanography*, *38*(3), 624–638. <https://doi.org/10.1175/2007JPO3798.1>
- Thomas, L. N. (2008). Formation of intrathermocline eddies at ocean fronts by wind-driven destruction of potential vorticity. *Dynamics of Atmospheres and Oceans*, *45*(3-4), 252–273. <https://doi.org/10.1016/j.dynatmoce.2008.02.002>
- Trott, C. B., Subrahmanyam, B., Chaigneau, A., & Delcroix, T. (2018). Eddy tracking in the northwestern Indian Ocean during southwest monsoon regimes. *Geophysical Research Letters*, *45*(13), 6594–6603. <https://doi.org/10.1029/2018GL078381>
- Trott, C. B., Subrahmanyam, B., & Murty, V. S. N. (2017). Variability of the Somali Current and eddies during the southwest monsoon regimes. *Dynamics of Atmospheres and Oceans*, *79*, 43–55. <https://doi.org/10.1016/j.dynatmoce.2017.07.002>
- Williams, S., Petersen, M., Bremer, P. T., Hecht, M., Pascucci, V., Ahrens, J., et al. (2011). Adaptive extraction and quantification of geophysical vortices. *IEEE Transactions on Visualization and Computer Graphics*, *17*(12), 2088–2095. <https://doi.org/10.1109/TVCG.2011.162>
- Yi, J., Du, Y., He, Z., & Zhou, C. (2014). Enhancing the accuracy of automatic eddy detection and the capability of recognizing the multi-core structures from maps of sea level anomaly. *Ocean Science*, *10*(1), 39–48. <https://doi.org/10.5194/os-10-39-2014>
- Zhang, Z., Yu, Z., & Wei, W. (2016). Three-compartment structure of subsurface-intensified mesoscale eddies in the ocean. *Journal of Geophysical Research: Oceans*, *122*, 1653–1664. <https://doi.org/10.1002/2016JC012376>
- Zhurbas, V., Stipa, T., Malkki, P., Paka, V., Golenko, N., Hense, I., & Sklyarov, V. (2004). Generation of subsurface cyclonic eddies in the southeast Baltic Sea: Observations and numerical experiments. *Journal of Geophysical Research*, *109*, C05033. <https://doi.org/10.1029/2003JC002074>